Low-Cost Hybrid Additive Manufacturing of a Miniaturized Dual Band Stacked Patch Antenna for GNSS Applications

Hehenberger, Simon; Caizzone, Stefano; Yarovoy, Alexander

DOI
10.23919/EuCAP60739.2024.10501211

Publication date
2024

Document Version
Final published version

Published in
Proceedings of the 2024 18th European Conference on Antennas and Propagation (EuCAP)

Low-Cost Hybrid Additive Manufacturing of a Miniaturized Dual Band Stacked Patch Antenna for GNSS Applications

Simon P. Hehenberger*†, Stefano Caizzone*, Alexander Yarovoy†
*Institute for Communication and Navigation, German Aerospace Center (DLR), Wessling, Germany, simon.hehenberger@dlr.de
†Microwave Sensing, Signals and Systems, Delft University of Technology, Delft, Netherlands

***Abstract*—The utilization of low-cost hybrid additive manufacturing equipment for creating a fully integrated patch antenna system is demonstrated. A miniaturized stacked dual-band patch antenna for GNSS applications with integrated feed, amplifier, matching, and bias network is considered. Design and manufacturing challenges due to the peculiarities of hybrid additive manufacturing, like anisotropic substrates, thermal curing steps, and poor layer adhesion between different materials, are discussed, and solutions are proposed. In this work, the passive part of the antenna is manufactured, and its measured performance is compared to results obtained via numerical simulations. An excellent agreement between simulation and measurement of the passive antenna is observed. The results of the fully integrated and active antenna will be demonstrated at the conference.**

***Index Terms*—patch antenna, dual band, additive manufacturing, 3D printing, GNSS**

I. Introduction

In recent years, additive manufacturing of high-frequency components such as antennas, lenses, and metamaterials has attracted increasing attention from researchers in the microwave community [1][2]. So far, the degrees of freedom offered by additive manufacturing have been employed to engineer purely dielectric devices such as dielectric resonator antennas [3][4], graded index lenses [5], or purely metallic devices such as horn antennas [6], slotted waveguide antennas [7], and metallic lenses [8]. A commonly employed hybrid approach is the metallization of printed dielectric parts via electroplating to create intricate, lightweight metallic parts [9]. However, this approach does not allow spatially metalizing printed parts, limiting its use case to fully metalized parts. Recently, additive manufacturing technology matured enough to enable the combined selective deposition of dielectric and conductive materials in the same process, allowing the additive manufacturing of circuits, antenna structures, and metamaterials [10] [11]. A particularly appealing hybrid additive manufacturing method is fused filament fabrication (FFF) combined with an extrusion system for conductive silver or copper ink/paste. However, materials available for FFF are usually optimized for printability, optical appeal, or mechanical properties rather than low-loss for high-frequency applications. Furthermore, issues of hybrid FFF in general, such as poor accuracy and low maximum temperature ratings of printed materials, limit the upper frequency and environmental compatibility of FFF 3D-printed antenna systems. Additional research about low-loss dielectric materials with high-temperature ratings and stability is necessary to exploit the potential of additive-manufactured antennas fully. Nevertheless, hybrid additive manufacturing already offers a compelling value proposition, providing opportunities for customization, performance enhancement, cost efficiency, and sustainability for low to mid-volume antenna system manufacturing.

In this work, we employ a low-cost, custom built, multi-tool FFF printing machine equipped with several filament extruders and a conductive silver ink dispensing system to demonstrate the manufacturing of an integrated dual-band stacked patch antenna. The design, inspired by [13], is intended for the reception of right-hand circular (RHC) polarized GNSS signals in the E1 (1.575 GHz) and E5a (1.179 GHz) bands respectively. The antenna in its final form shall be miniaturized via high-permittivity dielectric materials and integrated with a low noise amplifier (LNA), appropriate matching and DC bias networks, as well as a coaxial connector as depicted in Figure 1. The goal is to manufacture the complete antenna system in a single process, combining different dielectric materials for the individual substrates and conductive silver ink for the patches, connections, and transmission lines between the components and connector.

The paper is structured as follows. In Section 2, we discuss the design in more detail while separating the design into the passive dual-band patch antenna and the integrated circuit part. Section 3 elaborates on the unique challenges faced upon preparing the design for single-process manufacturing and how the design is adapted to be compatible with the limitations of our materials and manufacturing system. Section 4 presents the simulation and measurement results concerning S-parameters and realized gain radiation patterns. Furthermore, the degradation of the antenna efficiency due to the utilized print materials is studied via the reduction in realized gain at the zenith. Conclusions are drawn in Section 5.

II. Design

To explain the proposed design further, we refer to the stack-up depicted in Figure 2. Furthermore, we split the design into the antenna and circuit parts, as indicated in Figure 1 and discuss the individual parts separately below. Although the

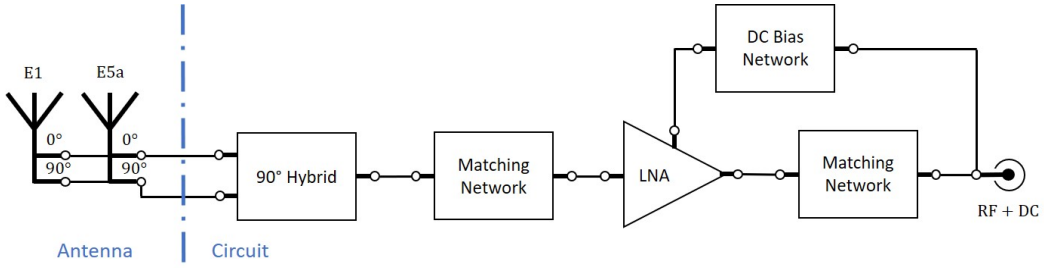

Fig. 1. Top level schematic of a dual band GNSS antenna with feed network and low noise amplifier.

circuit part is not the focus of this work, some details are provided to give a more complete picture of the work.

A. Antenna

The design employed in this work is inspired by the antenna introduced in [13], which consists of three layers of RO6010 ($\varepsilon_\mathrm{r} = 10.2$, $\tan\delta = 0.0023$) substrate with an upper and lower patch operating at the Galileo E1 and E5a center frequencies respectively. The individual patches are fed with proximity feeding from a probe extending vertically through the substrate layers, excited by a coaxial connector. The pins are terminated with a circular disk with radius r_cp to compensate for the feeding pin inductance and fine-tune the matching of the antenna. In this work, we extend the design from [13] with a feed and amplifier network and adapt it for compatibility with our available materials and additive manufacturing system. Figure 2 depicts a schematic of the stack-up. The RO6010 substrate from the original design is replicated via the Avient (former PrePerm) ABS1500 filament, a commercially available, high-permittivity ($\varepsilon_\mathrm{r} = 15$, $\tan\delta = 0.018$), thermoplastic material compatible with standard FFF machines. The integration of the 90° hybrid, the LNA, and the matching and DC bias networks will be done on a substrate printed with the Avient ABS300 filament, which exhibits a lower permittivity ($\varepsilon_\mathrm{r} = 3$, $\tan\delta = 0.018$) compared to the ABS1500 material. Conductive parts like the E1 and E5 patches and the circuitry connecting the LNA, 90° hybrid, and coaxial connector shall be done with the integrated dispensing system utilizing Elantas conductive silver ink Bectron CP 6662, which exhibits a moderate viscosity and a sheet resistivity of about 10 mΩ/sq/mil.

B. Circuit

The antenna is fed via two probes, excited with a phase offset of 90°, for sensitivity to RHC polarized signals. One could consider integrating the hybrid via a branch line coupler in stripline transmission lines. However, the branch line coupler does not obtain enough bandwidth to cover both the E1 and E5a bands with acceptable amplitude and phase unbalance. Therefore, we intend to utilize the dedicated wideband integrated hybrid for GNSS applications HC125A from Taoglas. Furthermore, we intend to utilize the wideband two-stage QPL9065 LNA from Quorvo for our design with the suggested matching and bias networks from its datasheet.

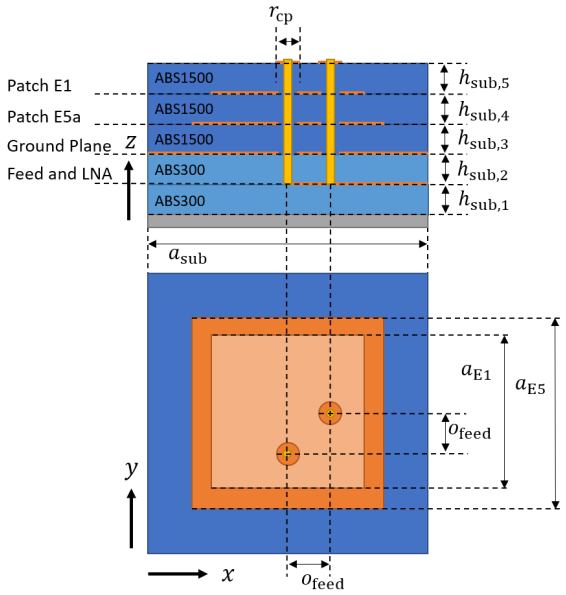

Fig. 2. The antenna design stack-up consists of five layers. Three high-permittivity material (ABS1500) layers are used to implement the miniaturized patches, and two low-permittivity materials (ABS300) are used to integrate the feed hybrid and LNA.

III. Design Challenges

The design introduced above is relatively straightforward. However, several particularities of the manufacturing process need to be considered during the design of the model and the print preparation to ensure accurate simulations and good printability. These particularities and their implications for the model and manufacturability are discussed in the following.

A. Print Setup and Settings

The final process incorporates three distinct materials. A high permittivity material for the patch substrates to achieve miniaturization, a lower permittivity substrate on which the feed, the 90° hybrid, the LNA, and further passive components are integrated, and conductive silver ink to fabricate the patches and transmission lines on their respective substrates. The print is carried out via a customized 3D printer based on the E3D tool changer, equipped with two Hemera extruders for the dielectric materials and the continuous dispensing equipment ViproHead from the manufacturer ViscoTech for the

TABLE I
MATERIAL PRINT SETTINGS

Material	**ABS300**	**ABS 1500**	**Bectron CP 6662**
Nozzle size	0.4mm	0.4mm	0.15mm
Nozzle temp.	280°C	230°C	-
Bed temp.	105°C	105°C	105°C
Max speed	$20\text{mm}\,\text{s}^{-1}$	$15\text{mm}\,\text{s}^{-1}$	$10\text{mm}\,\text{s}^{-1}$
Max acceleration	$400\text{mm}\,\text{s}^{-2}$	$400\text{mm}\,\text{s}^{-2}$	$100\text{mm}\,\text{s}^{-2}$
Layer height	0.12 mm	0.12 mm	0.04 mm

conductive ink material. The print settings for the individual materials are provided in Table I.

B. Substrate Material

Usually, FFF printing processes create the part layer-by-layer by extruding parallel lines with consecutive layers rotated 90° with respect to each other. A significant drawback of FFF is that tiny air inclusions on the edges of extruded lines are impossible to avoid. Therefore, printed parts will exhibit a reduction in permittivity from the nominal filament material parameters [14]. Furthermore, due to the layer-by-layer build approach, dielectric anisotropy is introduced into the printed substrate, which needs to be taken into account to predict the antenna performance [15] accurately. To achieve an accurate simulation of the antenna, the anisotropic permittivity of both the ABS1500 and ABS300, printed with settings provided in Table I, are measured with a quadratic aperture waveguide system in the X-band as explained in [15]. Measurement results for the complex permittivity tensor are depicted in Figure 3, and the averaged real-valued permittivity tensors are

$$[\varepsilon_{\text{r,ABS300}}] = \begin{bmatrix} 2.95 & 0 & 0 \\ 0 & 2.95 & 0 \\ 0 & 0 & 2.86 \end{bmatrix} \tag{1}$$

and,

$$[\varepsilon_{\text{r,ABS1500}}] = \begin{bmatrix} 12.75 & 0 & 0 \\ 0 & 12.75 & 0 \\ 0 & 0 & 10.9 \end{bmatrix}. \tag{2}$$

The negative values of the imaginary permittivity for the ABS300 in Figure 3b around 8.7GHz are physically not realistic and most likely due to imperfect calibration of the waveguide measurement system. For accurate loss characterization, a different approach, for example, a resonator system, would be more applicable. From the extracted material permittivity tensor values in (1) and (2), we can see that the layer-by-layer buildup results in a uniaxial anisotropic material with negative birefringence. The degree of anisotropy depends heavily on print settings and print setup quality [15]. The material characterization is carried out in the X-band, while the antenna is intended to operate in the L-band, which presents a potential source of error in the antenna design. However, according to the material supplier, the bulk material properties of the ABS1500 are stable up to 220GHz, and the periodicity of the printed lines is small enough that dispersion due to the

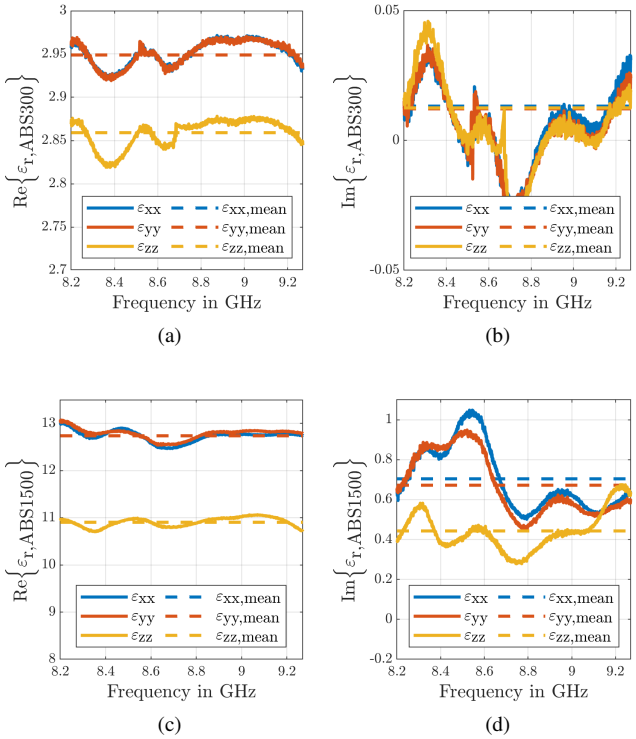

Fig. 3. Complex permittivity tensor measurement results of FFF manufactured samples (a)/(b) real/imaginary part ABS300 and (c)/(d) real/imaginary part ABS1500.

periodically structured material is negligible. Therefore, we are confident that the permittivity tensor values translate well between the two frequency bands.

C. Dielectric - Conductive Interface

The flatness of interfaces between dielectric and conductive materials is critical to ensure proper correspondence between the model considered in simulations and the manufactured part. Therefore, the surface onto which the utilized silver ink is dispensed should be as flat and smooth as possible to prevent the ink from leaking into the grooves between individually extruded lines. In this work, we utilize a layer post-processing technique called ironing to achieve a smooth surface. Ironing involves using a heated smoothing tool to apply controlled heat and pressure to the top surface of a 3D printed part, resulting in a smooth surface finish onto which the conductive ink can be dispensed.

D. Conductive Material

After dispensing, the Bectron CP 6662 silver ink requires thermal curing to reach the advertised conductivity. Curing is easily achieved by simply pausing the print and setting the heated bed to the desired curing temperature (120 °C for 10 minutes). The surface resistivity after thermal curing was measured with a four-point-probe system Jandel RM3-AR from Polytech GmbH to be about $\rho_s = 12$ mΩ/sq for a layer height of 40µm, corresponding well to the value reported in the datasheet of the ink (10 mΩ/sq/mil).

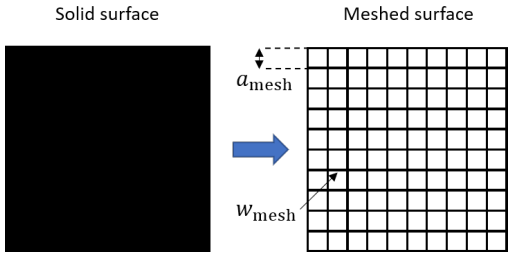

Fig. 4. Meshing solid conductive surfaces solves layer adhesion issues when printing on top of conductive silver ink.

E. Patch and Ground Plane Geometry

Upon first printing tests with dielectric and conductive ink, we experienced layer adhesion issues when attempting to print another layer of dielectric material onto a surface of conductive ink. Several adaptations of print settings were tested to resolve the issue with no success. To solve the issue of layer adhesion on conductive ink surfaces, we propose to utilize meshed surfaces. Figure 4 shows how a solid surface is replaced by a quadratic mesh with geometric parameters a_{mesh} and w_{mesh}. The meshing of the surface produces tiny "islands" of substrate material onto which the material of the next layer can attach itself. As long as the mesh density a_{mesh} is small enough w.r.t. the wavelength, the impact on the electromagnetic performance is negligible.

F. Feed and LNA Circuit

The glass transition temperature[1] of the utilized dielectric materials is about $120°\text{C}$. Therefore, commonly utilized soldering techniques are not applicable in order to create mechanical stable and conductive connections between the dispensed conductive silver ink and the terminals of the $90°$ hybrid or the LNA. To circumvent high-temperature soldering techniques, we utilize a two-component conductive epoxy (Distrelec CW2480) in order to create mechanically stable and conductive connections between the dispensed conductive silver and discrete components.

IV. Simulation and Measurement

After considering all the peculiarities discussed above, a model of the stacked patch is built in Ansys HFSS for numerical simulation and optimization. In this preliminary version of the paper, we only consider the upper three layers of the stack shown in Figure 2 mounted on a $100 \times 100\ \text{mm}^2$ aluminum ground plane. The results of integrating the feed, the $90°$ hybrid, and the LNA will be shown at the conference.

The model of the upper three high-permittivity layers together with the aluminum ground plane models the dielectric material with a permittivity tensor according to (2) and a loss tangent of $\tan\delta = 0.018$ provided by the datasheet of the material. Furthermore, the model considers the meshed surfaces for the E1 and E5a patches and the measured sheet resistivity of the conductive silver ink. The substrate heights $h_{\text{sub,5}}$, $h_{\text{sub,4}}$ and $h_{\text{sub,3}}$ are assigned to be $2.48\ \text{mm}$. Appropriate dimensions a_{E1} and a_{E5} of the patches for resonance at the E1 and E5a bands respectively are found via a parameter sweep and the antenna is matched by optimizing the offset of the feeds o_{feed}, and the radius of the coupling patches r_{cp}. All geometric dimensions of the final design are listed in Table II.

[1]At the glass transition temperature, the amorphous regions experience transition from rigid state to more flexible state marking the temperature at the border of the solid-state to rubbery state.

TABLE II
Geometric parameters of a dual-band stacked patch GNSS antenna optimized for operation in the Galileo E1 and E5a band, respectively.

Variable	Value	Variable	Value
a_{E1}	$23.6\ \text{mm}$	a_{E5}	$32.4\ \text{mm}$
$h_{\text{sub,3}}$	$2.48\ \text{mm}$	$h_{\text{sub,4}}$	$2.48\ \text{mm}$
$h_{\text{sub,5}}$	$2.48\ \text{mm}$	$o_{\text{feed,3}}$	$4.8\ \text{mm}$
r_{cp}	$2\ \text{mm}$	a_{sub}	$43\ \text{mm}$
a_{mesh}	$2\ \text{mm}$	w_{mesh}	$0.5\ \text{mm}$

The antenna is manufactured in a single process with print settings according to Table I and glued (3M adhesive 465) onto the aluminum ground plane. A SMA coaxial connector is mounted on the ground plane's backside with its inner pin extending vertically through the substrates and connected to the coupling patches via conductive epoxy. The assembled antenna is depicted in Figure 5a. The antenna is characterized in terms of its reflection coefficient and radiation pattern via measurement in an MVG Starlab antenna measurement chamber. Measurement results are depicted in Figure 5b. Furthermore, the impact of the print materials on the antenna's efficiency is studied by comparing the realized gain at zenith for the lossless, dielectric losses only, conductive losses only, and combined losses via simulations.

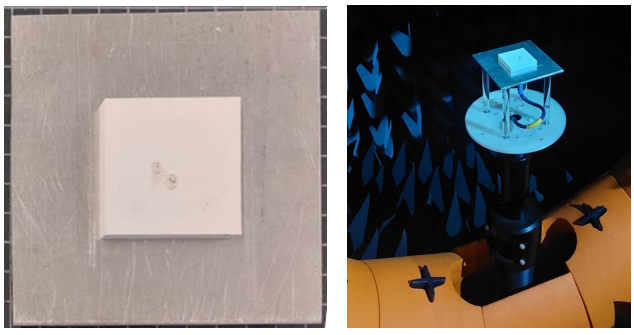

(a) (b)

Fig. 5. (a) Finished 3D printed stacked patch antenna for GNSS applications mounted on an aluminum ground plane. (b) Mounting of the antenna in an MVG Starlab anechoic chamber.

Comparison of the simulated and measured S-parameters in Figure 6a shows a resonance shift in the measured data of the lower band to higher frequencies. The resonance shift stems from the glue used to mount the antenna on the aluminum ground plane not being considered in the original design and

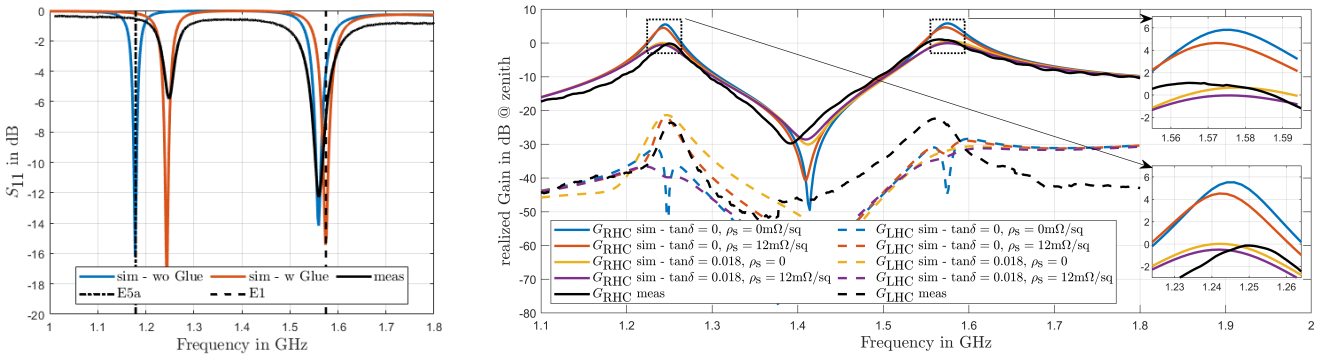

(a) S-parameters

(b) Realized Gain

Fig. 6. Comparison between simulation and measurement of the 3D printed stacked patch antenna (a) S-parameter, (b) realized gain at broadside. While (a) shows simulations with and without the glue to explain the shift in resonance frequency, (b) only considers simulation results with glue for better readability.

optimization. A post-manufacturing simulation, considering the glue, accurately predicts this resonance shift and shows a satisfying agreement between simulation and measurement. Comparison of the simulated realized RHC gains at zenith in Figure 6b shows an ≈ 1 dB drop in realized gain due to the finite conductivity of the Bectron CP6662 silver ink and an ≈ 5 dB drop due to the loss tangent of the ABS1500 material. One is able to observe a reasonable agreement between the simulated and measured realized gain values. Discrepancies might be explained by improper material parameter characterization since the conductivity of the silver ink was measured at DC conditions, and the permittivity tensor characterization was carried out in a frequency band different from the antenna's intended operating frequency.

V. Conclusion

In this work, we demonstrate the additive manufacturing of a miniaturized stacked patch antenna for GNSS applications via low-cost hybrid fused filament fabrication. Several peculiarities of hybrid FFF manufacturing techniques, such as uniaxially anisotropic substrates, layer adhesion issues when printing on top of dispensed conductive silver ink surfaces, in-process thermal curing of conductive ink, and integration of commercial off-the-shelf components, are addressed. A standalone passive dual-band antenna prototype has been optimized for operation in the E1 and E5a bands and manufactured with a custom hybrid additive manufacturing system. The effect of the print materials' finite conductivity and dielectric loss tangent is studied via numerical simulations, and an excellent agreement between measured and simulated performance is observed. The final, fully printed design, integrated with feed hybrid and amplifier, will be demonstrated at the conference.

References

[1] E. S. Rosker, R. Sandhu, J. Hester, M. S. Goorsky, and J. Tice, 'Printable materials for the realization of high performance RF components: Challenges and opportunities', Int. J. Antennas Propag., vol. 2018, pp. 1–19, 2018.

[2] T. Whittaker, S. Zhang, A. Powell, C. J. Stevens, J. Y. C. Vardaxoglou, and W. Whittow, '3D Printing Materials and Techniques for Antennas and Metamaterials: A survey of the latest advances', IEEE Antennas Propag. Mag., vol. 65, no. 3, pp. 10–20, Jun. 2023.

[3] Q. Lamotte et al., 'Multi-permittivity 3D-printed ceramic dual-band circularly polarized dielectric resonator antenna for space applications', in 2021 15th European Conference on Antennas and Propagation (EuCAP), Dusseldorf, Germany, 2021.

[4] S. P. Hehenberger, S. Caizzone, and A. G. Yarovoy, 'Additive manufacturing of linear continuous permittivity profiles and their application to cylindrical dielectric resonator antennas', IEEE Open J. Antennas Propag., vol. 4, pp. 373–382, 2023.

[5] J. W. Allen and B.-I. Wu, 'Design and fabrication of an RF GRIN lens using 3D printing technology', in Terahertz, RF, Millimeter, and Submillimeter-Wave Technology and Applications VI, San Francisco, California, USA, 2013.

[6] A. Sharma, R. K. Stilwell, S. Szczesniak, and C. Carpenter, '3D metal printed Ka-band quad-ridge horn antenna', in 2022 IEEE International Symposium on Antennas and Propagation and USNC-URSI Radio Science Meeting (AP-S/URSI), Denver, CO, USA, 2022.

[7] T. Van Trinh, J. Park, C. M. Song, S. Song, and K. C. Hwang, 'A 3-D metal-printed dual-polarized ridged waveguide slot array antenna for X-band applications', Appl. Sci. (Basel), vol. 13, no. 8, p. 4996, Apr. 2023.

[8] D. Shamvedi, P. O'Leary, and R. Raghavendra, 'Development of 3D printed metallic lenses', in 2023 17th European Conference on Antennas and Propagation (EuCAP), Florence, Italy, 2023.

[9] K. Lomakin et al., '3D printed slotted waveguide array antenna for automotive radar applications in W- band', in 2018 48th European Microwave Conference (EuMC), Madrid, 2018.

[10] D. Panusch, F. Hubert, F. Bachbauer, K. Lomakin, and G. Gold, 'Additively manufactured helix antenna for X-band applications', in 2022 16th European Conference on Antennas and Propagation (EuCAP), Madrid, Spain, 2022.

[11] K. H. Church et al., 'Multimaterial and multilayer direct digital manufacturing of 3-D structural microwave electronics', Proc. IEEE Inst. Electr. Electron. Eng., vol. 105, no. 4, pp. 688–701, Apr. 2017.

[12] M. Li, Y. Yang, F. Iacopi, J. Nulman, and S. Chappel-Ram, '3D-printed low-profile single-substrate multi-metal layer antennas and array with bandwidth enhancement', IEEE Access, vol. 8, pp. 217370–217379, 2020.

[13] S. Caizzone, 'Miniaturized E5a/E1 antenna array for robust GNSS navigation', IEEE Antennas Wirel. Propag. Lett., vol. 16, pp. 485–488, 2017.

[14] A. Goulas et al., 'The impact of 3D printing process parameters on the dielectric properties of high permittivity composites', Designs, vol. 3, no. 4, p. 50, Nov. 2019.

[15] S. P. Hehenberger et al., 'Dielectric Anisotropy in Materials Manufactured via Fused Filament Fabrication Processes', Material Research Bulleting (unpublished)